



AIAA 96-0937

**Rayleigh/Raman/LIF Measurements in a Turbulent
Lean Premixed Combustor**

S. P. Nandula and R. W. Pitz
Vanderbilt University
Nashville, TN

R. S. Barlow and G. J. Fiechtner
Sandia National Laboratories
Livermore, CA

**34th Aerospace Sciences
Meeting & Exhibit**
January 15-18, 1996 / Reno, NV

RAYLEIGH/RAMAN/LIF MEASUREMENTS IN A TURBULENT LEAN PREMIXED COMBUSTOR

S. P. Nandula* and R. W. Pitz†
Vanderbilt University
Department of Mechanical Engineering
Nashville, TN 37235

R. S. Barlow§ and G. J. Fiechtner§
Sandia National Laboratories
Combustion Research Facility
Livermore, CA 94566

Abstract

Simultaneous, time resolved measurements of major species (CH_4 , O_2 , N_2 , H_2 , H_2O , and CO_2), temperature, OH, NO, and CO are obtained in turbulent lean premixed methane-air flames, using a combination of Rayleigh scattering, spontaneous Raman scattering, and laser induced fluorescence (LIF). The measurements are performed in a bluff-body stabilized turbulent combustor burning premixed methane/air at an equivalence ratio of 0.586. Results show that the combustion in the recirculation zone is nearly complete and the reaction progress variable based on temperature $\{(T - T_0)/(T_{ad} - T_0)\}$ is 0.92. Radial profiles of species concentrations and temperature are uniform at all downstream locations in the recirculation zone. The species concentrations and temperature in the exhaust plane of the combustor (6 diameters downstream) are at adiabatic equilibrium. The NO concentrations in the exhaust plane of the combustor are small (~6 ppm), however the CO concentrations are relatively large (~1500 ppm). In the exhaust plane of the combustor, pollutants (NO and CO) are also measured with gas sampling probes. The probe and optical measurements of NO are in agreement, but the CO

measurements with an uncooled gas sampling probe are about 10 times smaller than the optical measurements.

Introduction

Much of the industrial electrical generation capability being added worldwide is gas-turbine engine based and is fueled by natural gas. These gas-turbine engines use lean premixed (LP) combustion to meet the strict NO_x emission standards. In conventional, diffusion flame gas turbine combustors, large amounts of NO_x are formed in the hot stoichiometric zones via the Zeldovich (thermal) mechanism. Hence, lean premixed combustors are rapidly becoming the norm, since they are specifically designed to avoid these hot stoichiometric zones and the associated thermal NO_x . Although LP combustion is an effective way to control NO_x , often it results in increased CO emissions. With the environmental regulatory challenges of NO_x reduction to the goal of under 10 ppmvd,¹ while maintaining acceptable levels of CO, research on NO_x and CO emissions has become a high priority. Achieving this objective would require extensive experiments in LP CH_4 flames for understanding the combustion phenomena underlying the formation of the exhaust pollutants. The formation and destruction of the pollutants (NO_x and CO) are strongly affected by the fluid mechanics, the finite-rate chemistry, and their (turbulence-chemistry) interactions. Hence, a thorough understanding of these interactions is vital for controlling and reducing the pollutant emissions. The present research is contributing to this goal by providing a

* Graduate Student, Student Member, AIAA.

† Professor, Senior Member, AIAA.

§ Member, AIAA.

Copyright © 1996 by S. P. Nandula. Published by the American Institute of Aeronautics and Astronautics with permission.

detailed nonintrusive laser based data set with good spatial and temporal resolutions of the pollutants (NO and CO) along with the major species, temperature, and OH. The measurements reported in this work, along with the existing velocity data² on the turbulent combustor burning CH₄, would provide insight into the turbulence-chemistry interactions and their effect on pollutant formation.

In turbulent flames, sensitive laser-based nonintrusive measurements of NO_x and CO are very limited, primarily due to the difficulty in measuring small concentrations (~ppm) of CO and NO. Previous experimental studies of NO_x and CO formation have been based almost entirely on gas-sampling probe techniques.³⁻⁵ However, the *instantaneous* relationships between the pollutants and the other scalars that are crucial for evaluating the turbulence-chemistry interactions are lost, since the gas sampling probes provide only averaged measurements. Hence, the data from probes has limited applicability for evaluation and refinement of engineering models of emissions.

Non-intrusive diagnostics based on spontaneous Raman scattering has been used successfully by previous researchers⁶⁻¹⁴ to obtain scalar (species and temperature) measurements in CH₄ flames. These measurements in CH₄ flames have provided a database for evaluation of combustion models and prediction of the turbulence-chemistry interactions.^{15,16} However, there are no simultaneous laser based multispectral measurements in premixed turbulent CH₄ flames that include the exhaust pollutants (NO and CO). The clear need for such measurements in methane flames, which would point the way to the effects of turbulence-chemistry interactions in NO and CO formation and guide the development of emissions models and perhaps, reduced chemistry schemes, has prompted this research.

Objectives

The objectives of the research were (i) to obtain simultaneous and instantaneous quantitative nonintrusive laser based measurements with good spatial and temporal resolutions; (ii) to provide insights into the role of the turbulence-chemistry interactions on pollutant (NO and CO) formation in turbulent LP methane-air flames; and

(iii) to provide a data base for evaluation and refinement of existing engineering models of emissions for gas-fired, lean premixed combustion turbines. The optical measurements include major species concentrations (CH₄, O₂, N₂, H₂O, H₂, CO₂), temperature, and OH along with the pollutants, NO and CO. In this paper, we present results of major species, temperature, OH, and the pollutants from a lean premixed bluff body stabilized turbulent combustor burning methane. Extensive measurements ranging from 0.1 diameters to 6 diameters downstream of the bluff body and from the center to 0.6 diameters radially outward were performed to map the flow field of the combustor. The combustor and the flame parameters were chosen to match the conditions for which Pan and co-workers have reported velocity and temperature measurements using Laser Doppler Anemometry and Coherent Anti-Stokes Raman Spectroscopy respectively.^{2,17-19} These multispectral measurements, along with the reported velocity measurements will provide insight into the NO_x and CO formation in the combustor.

Approach

The strategy for the Rayleigh/Raman/LIF measurements was as follows; spontaneous Raman scattering was used to obtain the quantitative single-pulse major species concentrations and the pollutant CO. In the present experiment (LP CH₄-air environment), the major species that were monitored were CH₄, O₂, N₂, H₂, H₂O, and CO₂. Temperature was determined from the strong Rayleigh scattering signal which was monitored simultaneously. The Rayleigh signal was converted to temperature by a species weighted scattering cross-section from the Raman measurements and the index of refraction data of Gardiner et al.²⁰ The minor species, OH and NO, were measured by separate lasers using linear (or near-linear) laser induced fluorescence. The LIF signals from the minor species (NO and OH) were then corrected on a single-shot basis for quenching (which is species and temperature dependent) and population fraction (which is temperature dependent), to obtain their quantitative values.²¹ Temperature was also obtained for each laser shot from the measurements of species concentrations by invoking the perfect gas law.

Diagnostic System

A schematic of the experimental system is shown in Fig. 1. The lean premixed combustor was mounted at the exit of a vertical wind tunnel which could be translated along the three axes. The beam from two Nd:YAG lasers (532 nm, ~750 mJ/pulse, 10 Hz) was used for Raman (major species and CO) and Rayleigh (temperature) measurements. This laser has a pulse length of 10 ns which was stretched to 150 ns to avoid laser induced breakdown at the focal volume. The LIF measurements of minor species (NO and OH) were accomplished with two separate Nd:YAG-pumped dye laser systems. The three laser beams were combined into a common axis, using two dichroic mirrors, and focused into the test section. The 532 nm beam was retroreflected into the measurement volume using a prism to effectively double the Rayleigh and Raman signals. The spatial resolution of the measurements was ~ 800 μm in each direction, and the delays between each of the three pulses were ~ 100 ns. The laser firing sequence was as follows; NO laser, followed by the OH laser and finally the 532 nm laser for Rayleigh/Raman measurements.

The scattered Raman and Rayleigh signals were collected using a six-element achromat and collimated using a conventional camera lens. The collimated light was relayed to photomultiplier tubes (PMT's) aligned at the exit plane of a 0.75-m spectrometer. Fluorescence signals from OH and NO were collected using Cassegrain optics located on the other side of the test section as shown in Fig. 1. A dichroic mirror separated and relayed the NO and OH fluorescence signals to separate detectors.

For OH excitation-detection, the frequency-doubled output for one of the dye lasers was tuned to the $O_{12}(8)$ transition in the $A^2\Sigma^+ - X^2\Pi(1, 0)$ band ($\lambda = 287.9$ nm). Colored glass filters were placed in front of the OH detector to capture much of the fluorescence from the dominant (1, 1), (1, 0), and (0, 0) bands, where the (0, 0) fluorescence is preceded by vibrational energy transfer. For NO excitation, the second dye laser was tuned to the $R_1(18)$ transition in the $A^2\Sigma^+ - X^2\Pi(0, 0)$ band. This state is reasonably isolated from the neighboring NO lines, and the ground state is populated over a wide range of temperatures, including room temperature. A solar-blind PMT (Hamamatsu R166) and Schott UG-5 colored glass

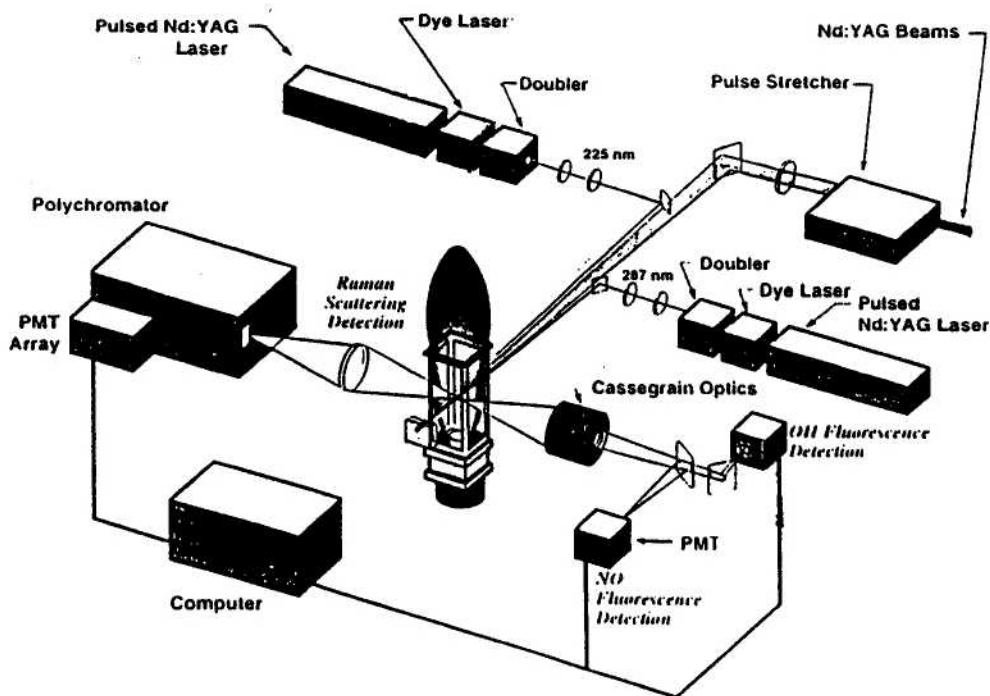


Fig. 1 Schematic of the Rayleigh/Raman/LIF diagnostic system.

filters were used for detection of NO signals. This arrangement allowed collection of fluorescence from the system of NO bands at 236, 247, 259, and 271 nm.

Wavelengths of the laser beams of NO and OH were each monitored indirectly by measuring fluorescence from two small premixed CH₄-air flames. Then during the course of the measurements, the two dye lasers were adjusted as necessary to remain line-centered on the NO and OH transitions. Detailed descriptions of the experimental system have been reported previously.²²

Signal Calibration

The diagnostic system was calibrated for temperature dependent calibration factors and cross-talk between the Raman channels, to convert the raw signals to absolute species concentrations and temperature. This was accomplished by measuring signals in nearly laminar adiabatic flames over a wide range of equivalence ratios. The O₂, N₂, H₂O, and H₂ Raman signals and the OH LIF signals were calibrated in H₂-air flames over an uncooled multi-element Hencken burner for equivalence ratios ranging from 0.2 (fuel lean) to 1.7 (fuel rich). The heat

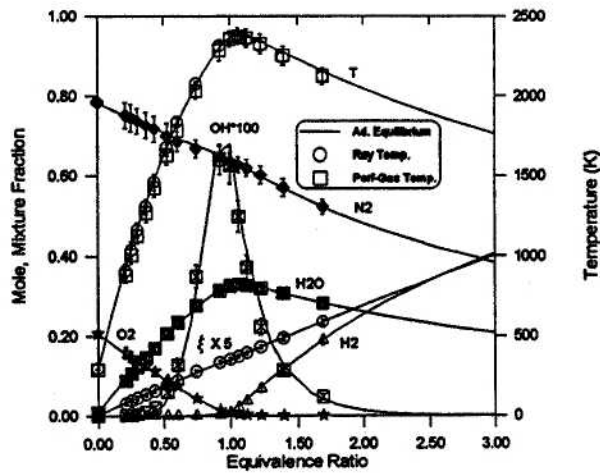


Fig. 2 Calibration results of the major species concentrations (O₂, N₂, H₂O, and H₂), OH, and temperature at various equivalence ratios in a laminar adiabatic H₂-air flame. The lines show calculations for a laminar equilibrium flowfield. The error bars denote the single-shot uncertainty ($\pm \sigma$) in the measurements.

loss from the burner is negligible at sufficiently high flowrates. The flowfield at this location (~4 cm downstream) is uniform and the species concentrations and temperature are at adiabatic equilibrium. The radiative heat losses in H₂-air flames for this burner are ~20-40 K. The calibration results of the species concentrations, temperature, and mixture fraction over a range of equivalence ratios are shown in Fig. 2. The lines in the figure show laminar adiabatic equilibrium calculations obtained using STANJAN.²³ The calibrations show good agreement with the theoretical equilibrium curves. The single-pulse relative standard deviations (\pm one standard deviation, σ) of species concentrations, temperature, and mixture fraction are shown as error bars in the figure.

Similar calibrations were performed in CH₄-air flames over the Hencken burner and are shown in Fig. 3. The Raman signals from O₂, N₂, H₂O, CO₂, CO and the LIF signals from OH were calibrated in this flame. The radiative heat losses in CH₄ flames in the burner are slightly higher (30-50 K) than those of the hydrogen flames due to the presence of CO₂. Thus temperature dependent calibration factors were derived for all the major species except CH₄. Methane decomposes readily even at moderate temperatures and no CH₄ is present even in rich CH₄ flames. Therefore, the calibration factor measured in CH₄/air flows at ambient temperature was used for calibrating the CH₄ Raman channel. This calibration constant for CH₄ was assumed to be independent of temperature.

The NO system was calibrated using laminar CH₄/N₂/O₂ flame ($\phi = 0.72$; $T = 1700$ K) over a McKenna burner. Naturally occurring NO concentrations in these flames are very small to allow concentration measurements by absorption. Hence, for reliable calibration measurements, these flames are doped with known concentrations of NO (~30 ppm) for calibration of the NO LIF system. The flame was chosen because the destruction of doped NO in these flames is small.²⁴ The OH and NO fluorescence signals in the turbulent flame are corrected on a shot-to-shot basis for variations in the Boltzman fraction and quenching rate as compared with the conditions. Detailed

descriptions of calibration procedures have been reported previously.²²

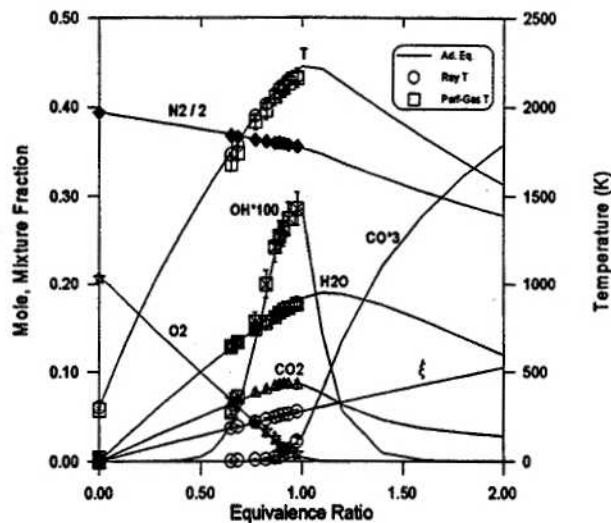


Fig. 3 Calibration results of the major species concentrations (O_2 , N_2 , H_2O , CO_2 , and CO), OH , and temperature at various equivalence ratios in a laminar adiabatic CH_4 -air flat flame. The lines show calculations for a laminar equilibrium flowfield. The error bars denote the single-shot uncertainty ($\pm \sigma$) in the measurements.

Measurement Uncertainty and Shot Noise

The single-shot uncertainties in the measurements were obtained from the measurements performed in the laminar adiabatic flames (Hencken/McKenna burners) which were used for system calibration. Typical uncertainties of the species concentrations and temperature are shown in Table 1. Most of the uncertainties shown in the table correspond to an equivalence ratio (ϕ) of 0.65. This equivalence ratio was chosen as the representative, as it is the closest of all the calibration flames, to the equivalence ratio of the LP CH_4 /air flame ($\phi = 0.586$) in the turbulent combustor. The uncertainties are primarily due to the shot noise resulting from the photoelectron emission process of the photocathode. However, these uncertainties also include contributions from the instrument noise and fluctuations in the flame conditions (due to burner nonuniformities). The single-shot uncertainty in the CO measurements is large (17.6%) compared to the other Raman measurements primarily due to the small number density of CO . Single-pulse uncertainties of species concentrations, temperature, and mixture fraction (ξ) over a range of equivalence ratios are shown in Figs. 2 and 3 as error bars ($\pm \sigma$).

Table 1
Typical Single-Pulse Uncertainties of the Measurements

Scalar	Burner	Fuel	ϕ	T (K)	No. Density (#/cm ³)	% rms
O_2	Hencken	CH_4	0.65	1754	0.28×10^{18}	7.5
N_2	"	"	"	1754	3.09×10^{18}	3.1
CH_4	"	Cold CH_4	0.10	300	2.60×10^{18}	3.3
H_2O	"	CH_4	0.65	1754	0.53×10^{18}	5.1
CO_2	"	"	"	1754	0.27×10^{18}	5.1
CO	"	"	0.98	2219	2.18×10^{16}	17.6
T_{ray}	"	"	0.65	1754	N/A	1
ξ	"	"	"	1754	N/A	4.1
OH	"	"	"	1754	1.83×10^{16}	10.5
NO	McKenna	$CH_4/N_2/O_2$	0.72	1700	1.3×10^{14}	7.6

In addition to these uncertainties, there is uncertainty in the CO measurements due to the cross-talk of the N₂ channel on the CO Raman channel. The vibrational hot bands of nitrogen interfere with the CO channel, resulting in an apparent CO signal. For instance, at an equivalence measurements in laminar H₂-air adiabatic flames (Hencken burner) and is subtracted from the CO channel during data processing. However, there is a 3.8% uncertainty in the measurement of this cross-talk, resulting primarily from the uncertainties in the measurement of N₂ number density, temperature, and the cross-talk calibration curve. These uncertainties translate into an uncertainty of ± 660 ppm in the single-shot measurements of CO at $\phi = 0.65$. These uncertainties in the CO measurements are representative of the uncertainties in the measurements on the turbulent LP combustor ($\phi = 0.586$).

The single-pulse uncertainties in LIF measurements of OH and NO are 10.5 and 7.6% respectively. In addition to these uncertainties, the LIF measurements are subject to systematic errors due to the wavelength drift of the dye lasers from the line center. The maximum resulting uncertainties due to the wavelength drift are estimated to be $\sim 5\%$ for OH and $\sim 10\%$ for NO. Furthermore, there is a systematic uncertainty of ~ 2 -3 ppm in the NO measurements due to the O₂ interference on NO. In the present set of experiments this interference was not accounted for during system calibration. Hence the mean measurements of NO could be higher than the actual NO concentrations by 2-3 ppm. The sensitivity of the NO LIF system is still sufficient to obtain useful measurements below 10 ppm.

LP Combustor and Flame Parameters

The schematic of the lean premixed combustor used for the experiments is shown in Fig. 4. Fuel (CH₄) and air are premixed ~ 3 m upstream and injected at the base of the combustor. The fuel/air mixture is not preheated and the temperature of the mixture is 300 K. Several screens and honeycombs are used to make the flow uniform and prevent flashback of the LP flame. A stainless steel conical bluff body of base diameter ($d = 44.45$ mm) and apex angle ($\theta = 45^\circ$) served as the flame holder. The

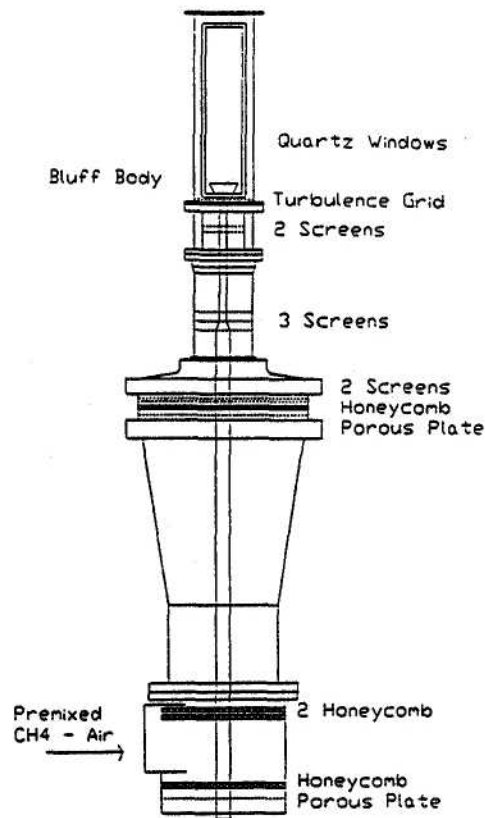


Fig. 4 Schematic of the bluff-body stabilized lean premixed CH₄-air turbulent combustor.

bluff body is mounted coaxially at the center of the 79 mm x 79 mm x 284 mm combustor test section. The blockage ratio, which is defined as the ratio of the area of the bluff body to the total base area, with this configuration is 25%. The test section has rounded corners with four 56.4 mm x 254 mm cutouts for mounting windows. Quartz windows are mounted on the signal receiving side of the diagnostic system. On the other side of the combustor section where the laser beams pass through, the quartz windows are replaced by windows made of high temperature resistant ($\sim 2000^\circ$ F) fiberfrax walls. This is because the energy density of the 532 nm YAG laser is higher than the damage threshold of the quartz windows. Small holes of 9.5 mm diameter are drilled through the fiberfrax to let the three laser beams to pass through. Holes of small diameter are chosen so that they would not significantly alter the flowfield in the combustor but let the laser beams to pass with sufficient clearance. A turbulence grid is

but let the laser beams to pass with sufficient clearance. A turbulence grid is placed at the entrance of the combustor section at 58 mm upstream of the bluff body. The reference velocity at the entrance of the test section in this configuration is 15 m/s, and the free stream turbulence is 24%. The combustor is mounted on a vertical wind tunnel contraction which can be traversed along three axes.

The flame parameters in the present experiment correspond to an air flow rate of 3960 slpm (standard liters per minute) and fuel (CH_4) flow rate of 244 slpm, resulting in an equivalence ratio of 0.586 and an adiabatic flame temperature (T_{ad}) of 1641 K. The air and fuel flow rates are identical to those used by Pan et al.² who measured velocity and temperature on the combustor.[†] The combustor produces a cone-stabilized premixed flame, which is shown in Fig. 5. The flame is stabilized by the bluff body (cone), with a recirculation zone which extends to ~ one diameter downstream, a shear layer or an annular flame zone, and a post flame zone. Rayleigh/Raman/LIF measurements are performed at various axial and radial locations on the combustor. In addition to the optical measurements, the pollutants (CO and NO) in the exhaust plane ($x/d = 6.0$) are measured with gas sampling probes. Table 2 summarizes the optical and gas sampling probe measurements. For

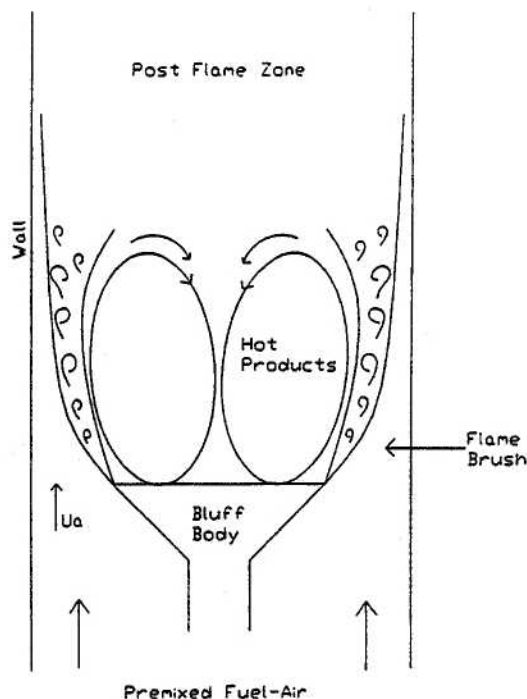


Fig. 5 Turbulent flame structure enveloping the recirculation zone of the bluff body stabilized combustor.

brevery, only measurements at locations shown in bold (see Table 2) are reported in this paper.

Table 2
Summary of optical and gas sampling probe measurements

Measurements	Streamwise location (x/d)
Optical Diagnostics (Major species [§] , temperature, CO, OH, and NO)	0.1, 0.3, 0.6, 0.8, 1.0, 1.2, 2.0, and 6.0 (exhaust plane)
Gas sampling probes (NO/NO ₂ and CO)	6.0 (exhaust plane)

§ Major species denote CO₂, CH₄, H₂, O₂, N₂, and H₂O.

[†] At these flowrates the equivalence ratio is 0.586 and not 0.65 as reported by Pan et al.²

Shadowing

Shadowing factors for the Raman, Rayleigh, and LIF signals are measured at each axial location, to account for the change in the solid angle of collection and obstruction of the signal due to the bluff body and/or the test section. Typical shadowing of the signals at 0.1 diameters downstream are shown in Fig. 6. It is evident from the figure that at radial locations greater than 0.50 diameters ($r/d > 0.5$), the optical signals decrease due to shadowing from the test section. A greater concern than the shadowing is the increase in the Rayleigh background at large r/d . The Rayleigh background is almost seven-fold at $x/d = 0.55$ relative to $x/d = 0$ (see figure). This Rayleigh background signal is primarily due to the surface scatter from the fiberfrax wall where the YAG laser clears the hole. The shadowing of the Raman/LIF signals and the increase in the Rayleigh background are a function of the axial location. Therefore, the shadowing factors are quantified at each location and accounted for during data processing.

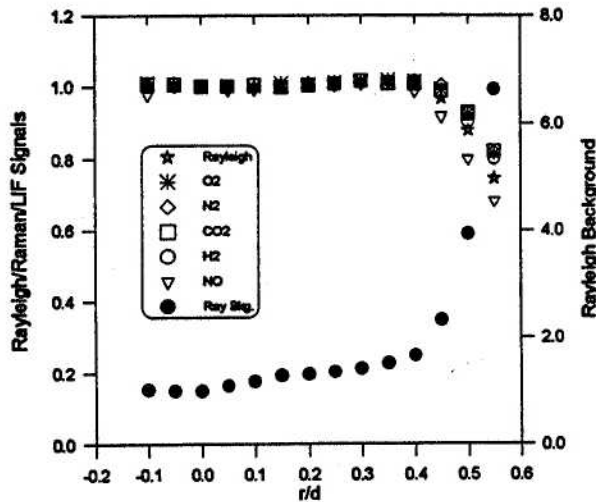


Fig. 6 Typical radial profiles of the Rayleigh/Raman/LIF shadowing factors and the Rayleigh background at $x/d = 0.1$.

Results and Discussion

Radial profiles of the average major species mole fractions, temperature, OH, CO, and NO at $x/d = 0.1$ are shown in Fig. 7. The bluff body and the quartz window (denoted as wall) are shown in the figure to facilitate the

physical visualization of the combustor. The equilibrium values of the species concentrations and temperature corresponding to the equivalence ratio (0.586) of the combustor are also shown. Typically 600-1000 laser shots were registered at each radial location. In the recirculation zone ($r/d < 0.5$), the mean values of the major species, temperature, OH, CO, and NO are radially uniform. The mean temperature in the recirculation zone (1540 K) is ~6% less than the adiabatic equilibrium temperature ($T_{ad} = 1641$ K). The reaction progress variable (C) based on temperature $\{(T - T_0)/(T_{ad} - T_0)\}$ is 0.925, where T_0 is the temperature of the premixed fuel/air at the entrance of the combustor (300 K). The reaction progress variable determines the degree of completion of the reaction; the reaction is frozen when the progress variable is zero and complete when the progress variable is 1. Hence, the combustion in the recirculation zone is ~92.5% complete. The NO and CO concentrations in the recirculation zone are about 10 ppm and 1000 ppm respectively. Hydroxyl (OH) concentrations are ~110 ppm and correspond to the adiabatic equilibrium value of LP CH₄/air flames at $T = 1540$ K.

At the edge of the bluff body ($r/d = 0.5$), next to the recirculation zone lies the thin shear layer. The presence of the shear layer can be seen from the hydroxyl (OH) profile which peaks sharply from 110 ppm in the recirculation zone to 175 ppm in the shear layer at $r/d = 0.5$. The shear layer thickness is estimated from the OH profile (see Fig. 7) and is ~4.45 mm ($r/d = 0.45-0.55$). The spatial resolution of the laser (~800 μ m) is not sufficient not resolve the thin shear layer of the premixed flame. Hence, there is spatial averaging in the data at the shear layer. The CO concentrations also peak in the shear layer and the average CO concentrations in the shear layer are ~5,300 ppm. Radially outward from the shear layer ($r/d > 0.5$), the temperature drops steeply from 1540 K to ambient (300 K). This cold region is characterized by the unburnt premixed fuel ($X_{CH_4} = 0.058$) and air ($X_{N_2} = 0.74$, $X_{O_2} = 0.192$) mixture which is injected at the base of the burner. The concentration of the products (H₂O and O₂) and the intermediate radicals (OH, CO, and NO) in this cold region are zero.

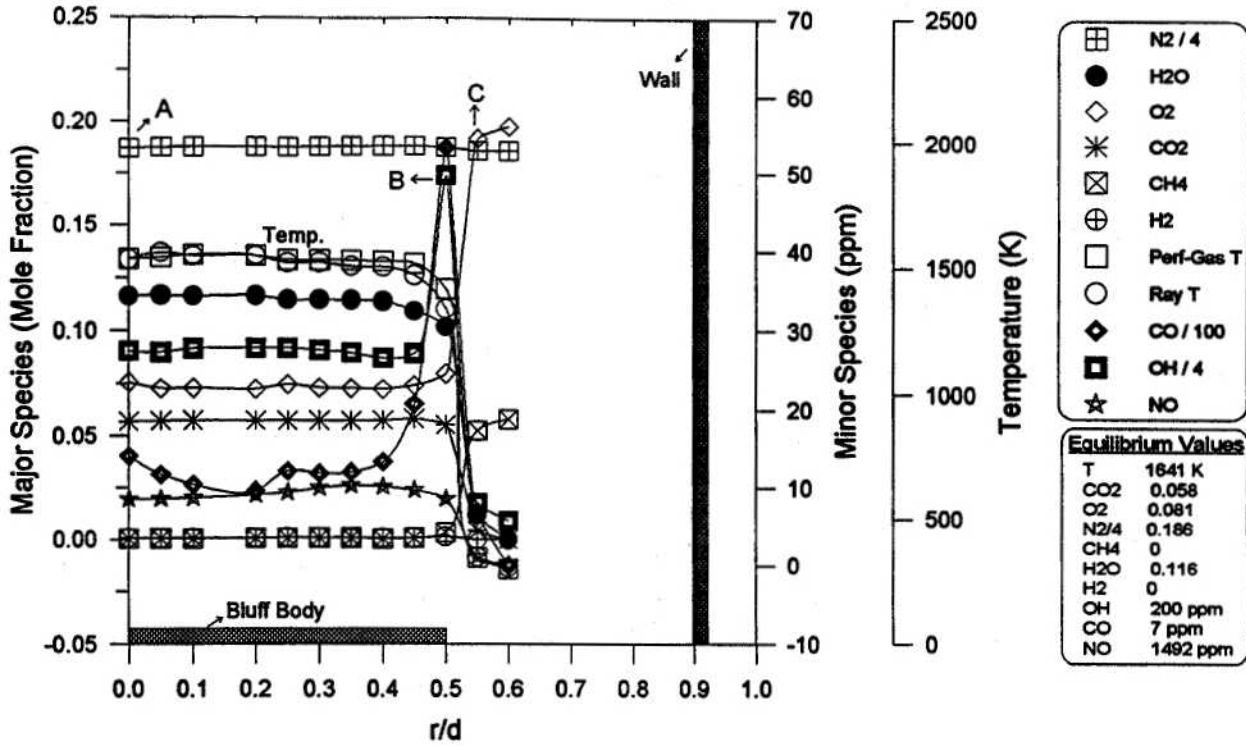


Fig. 7 Radial profiles of the mean species mole fractions and temperature at $x/d = 0.1$.

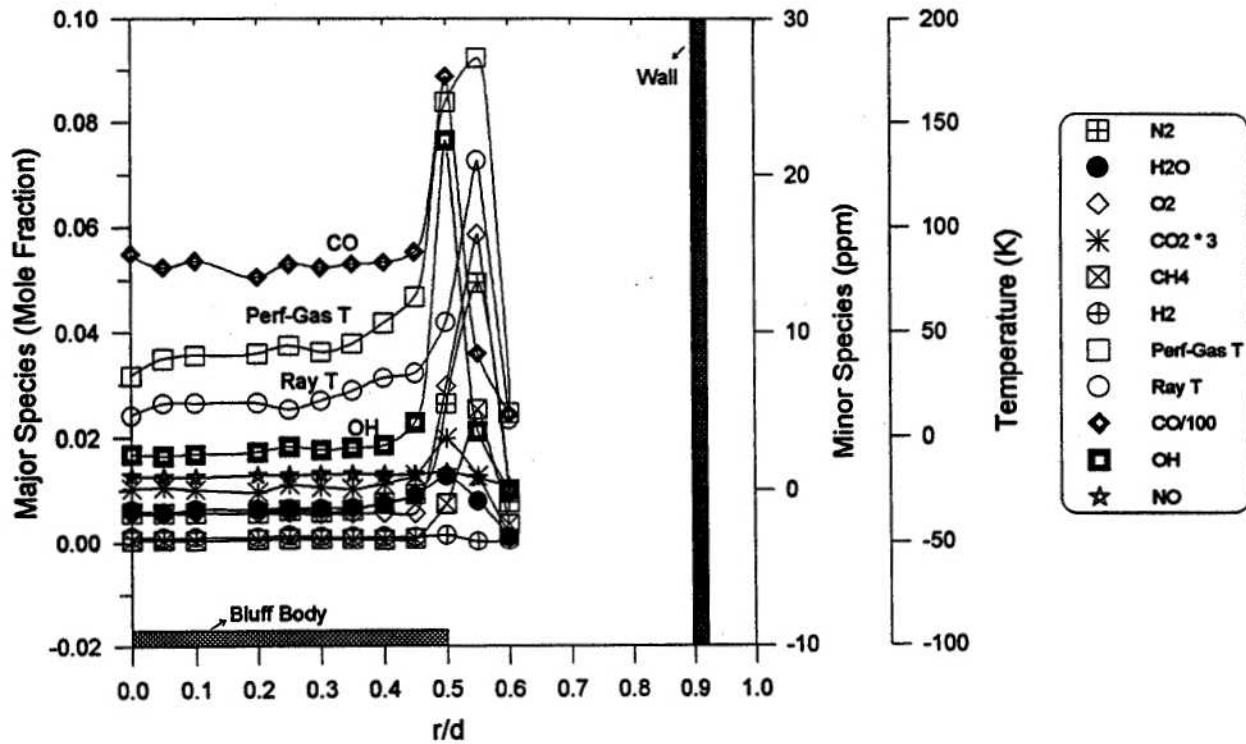


Fig. 8 Radial profiles of the rms species mole fractions and temperature at $x/d = 0.1$.

The radial profiles of the rms of the species and temperature are shown in Fig. 8. The rms of Rayleigh temperature is smaller than that of the perfect gas temperature (temperature calculated from the species concentrations by invoking the perfect gas law). This is primarily due to reduced shot noise in the strong Rayleigh signals as opposed to the Raman signals. The rms of CO even in the uniform recirculation zone is ~ 1400 ppm. The large value of the rms is primarily due to the photon shot noise of the weak CO Raman signals. The rms profiles are fairly uniform radially in the recirculation zone ($r/d < 0.5$). The radial profiles of the products (CO_2 and H_2O) and the intermediate radical species (OH and CO) peak in the shear layer at the edge of the bluff body ($x/d = 0.5$) as seen in Fig. 8. The profiles of fuel (CH_4), oxidizer (O_2 , N_2), and temperature peak slightly outward at $r/d = 0.55$, the region where the cold premixed fuel-air exchanges heat and mass to the shear layer.

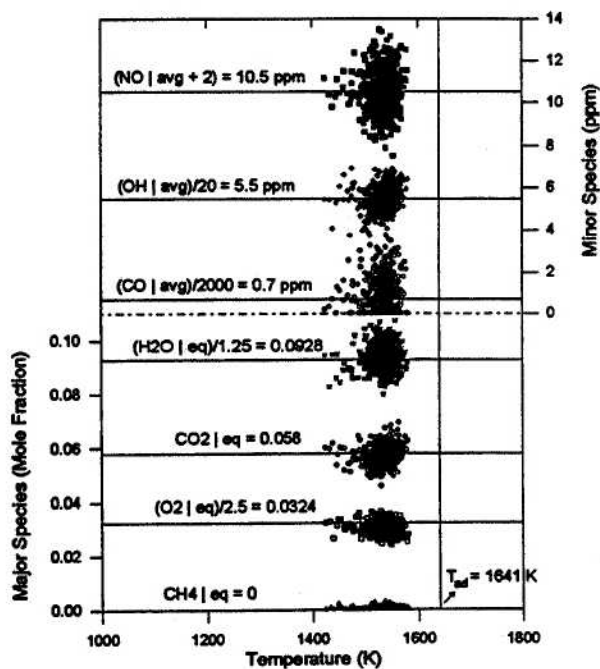


Fig. 9 Scatter plots of measured species mole fractions versus temperature in the combustor at $x/d = 0.1$ and $r/d = 0$ (Point A of Fig. 7). The equilibrium compositions of the major species corresponding to an equivalence ratio of 0.586 are shown as horizontal lines.

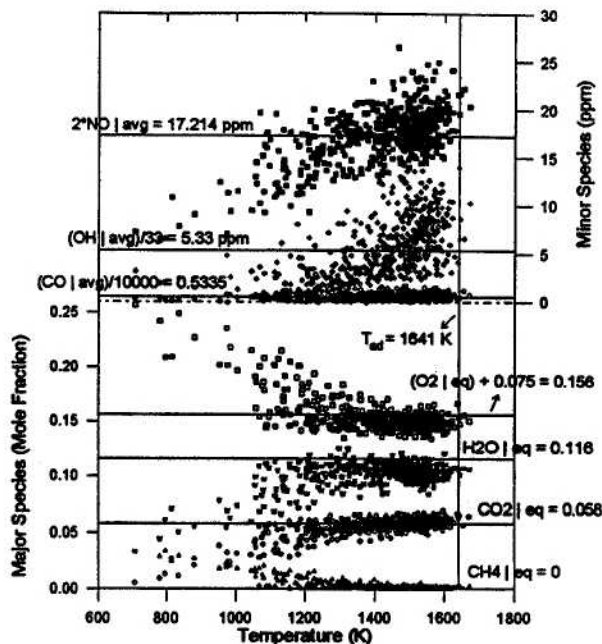


Fig. 10 Scatter plots of measured species mole fractions versus temperature in the combustor at $x/d = 0.1$ and $r/d = 0.50$ (Point B of Fig. 7). The equilibrium compositions of the major species corresponding to an equivalence ratio of 0.586 are shown as horizontal lines.

Scatter plots of the measured species mole fractions corresponding to points A, B, and C in Fig. 7 are plotted versus temperature and are shown in Figs. 9, 10, and 11 respectively. Figs. 9 and 10 are an ensemble of 600 laser shots and Fig. 11 is an ensemble of 1000 laser shots. Scatter plots such as these provide an overview of the chemistry as each point gives an instantaneous picture of the flame. The horizontal lines in the Figs. 9 and 10 are the adiabatic equilibrium values of the major species (CH_4 , O_2 , CO_2 , and H_2O) corresponding to an equivalence ratio of 0.586, and the average values of the minor species (CO, NO, and OH) at that location. The data in the recirculation zone (point A, $r/d = 0$, Fig. 9) is confined to a narrow temperature band (1425-1575 K). The major species mole fractions are scattered around the equilibrium values. The average CO, OH, and NO concentrations at this location are 1400 ppm, 110 ppm, and 8.5 ppm respectively.

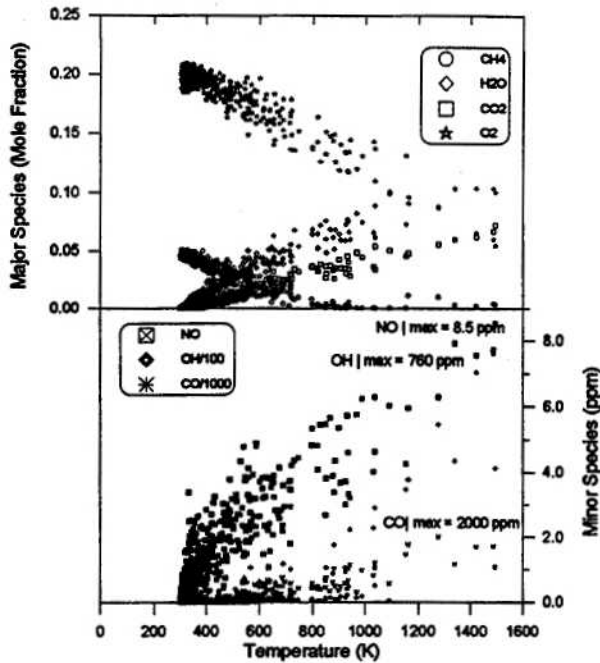


Fig. 11 Scatter plots of measured species mole fractions versus temperature in the combustor at $x/d = 0.1$ and $r/d = 0.55$ (Point B of Fig. 7). The equilibrium compositions of the major species corresponding to an equivalence ratio of 0.586 are shown as horizontal lines.

The instantaneous measurements in the shear layer (point B, $r/d = 0.5$) are shown in Fig. 10. The concentrations of the intermediate radicals (OH and CO) are considerably higher than their counterparts in the recirculation zone. The major species concentrations (CO_2 , H_2O , and O_2) are slightly below equilibrium. However, the peak OH concentrations are 475 ppm, more than twice the adiabatic equilibrium values (200 ppm) at $\phi = 0.586$. The CO concentrations (5400 ppm) are about 4 times their corresponding values in the recirculation zone (~1400 ppm). The scatter plot at the edge of the shear layer and the cold fluid (point C, $r/d = 0.55$, Fig. 11) lies over a broad range of temperature ranging from 300 K (ambient) to ~1550 K. This wide range of the instantaneous data is due to the turbulent mixing of the cold reactants with hot products in the shear layer. Superequilibrium OH concentrations (760 ppm), as high as 3.8 times the equilibrium values are recorded. The peak CO and NO concentrations are ~2,000 ppm and ~8.5 ppm respectively.

Mean radial profiles of the species concentrations, and temperature at $x/d = 0.3, 0.6,$ and 1.0 are shown in Figs.

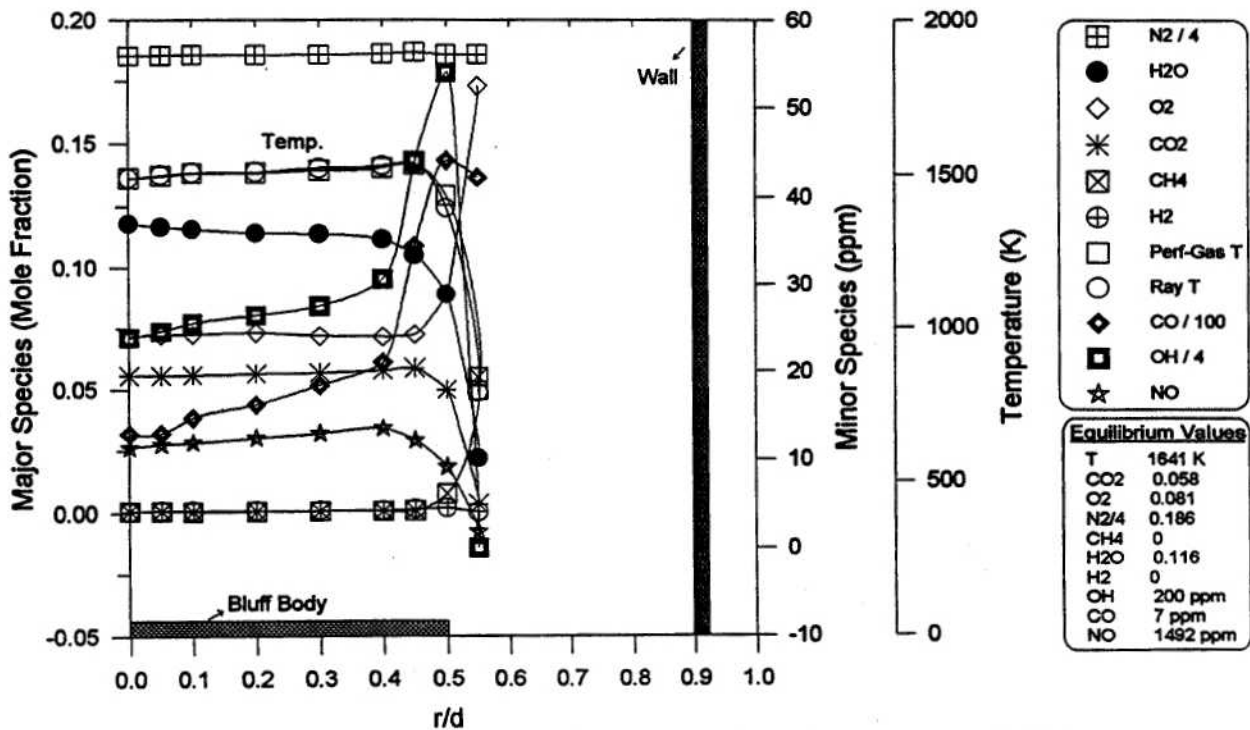


Fig. 12 Radial profiles of the mean species mole fractions and temperature at $x/d = 0.3$.

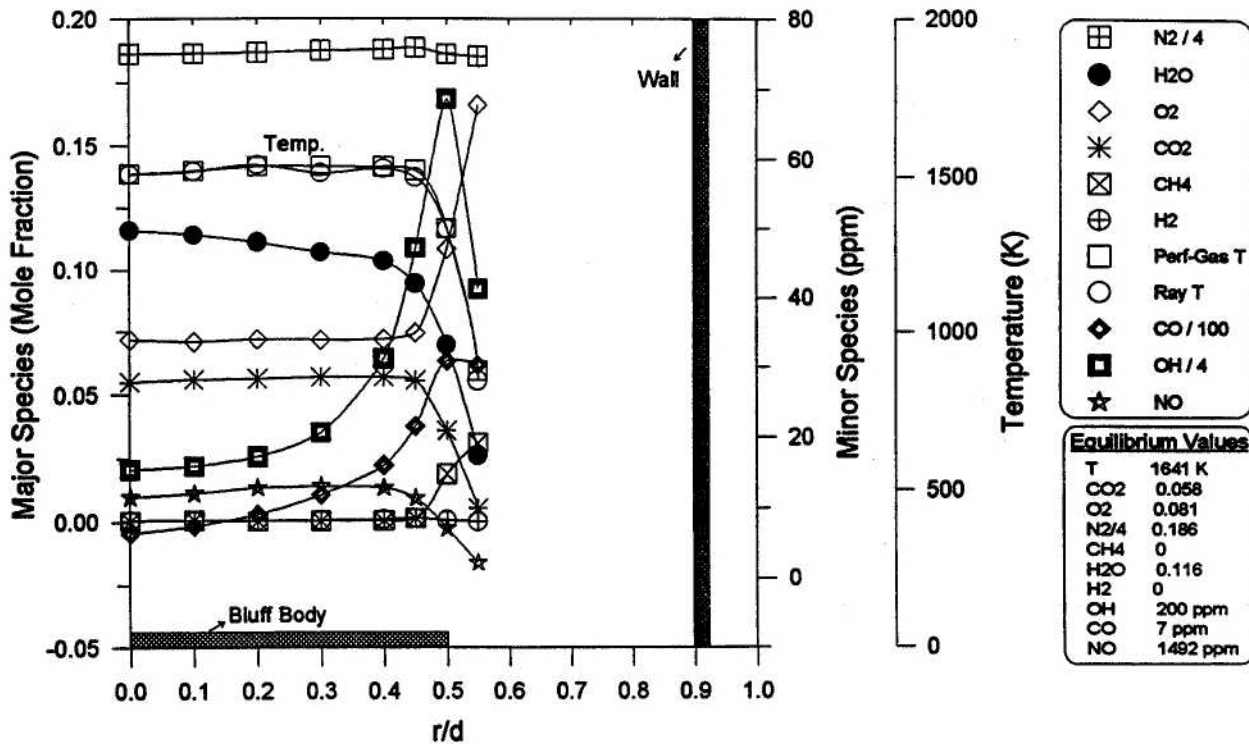


Fig. 13 Radial profiles of the mean species mole fractions and temperature at $x/d = 0.6$.

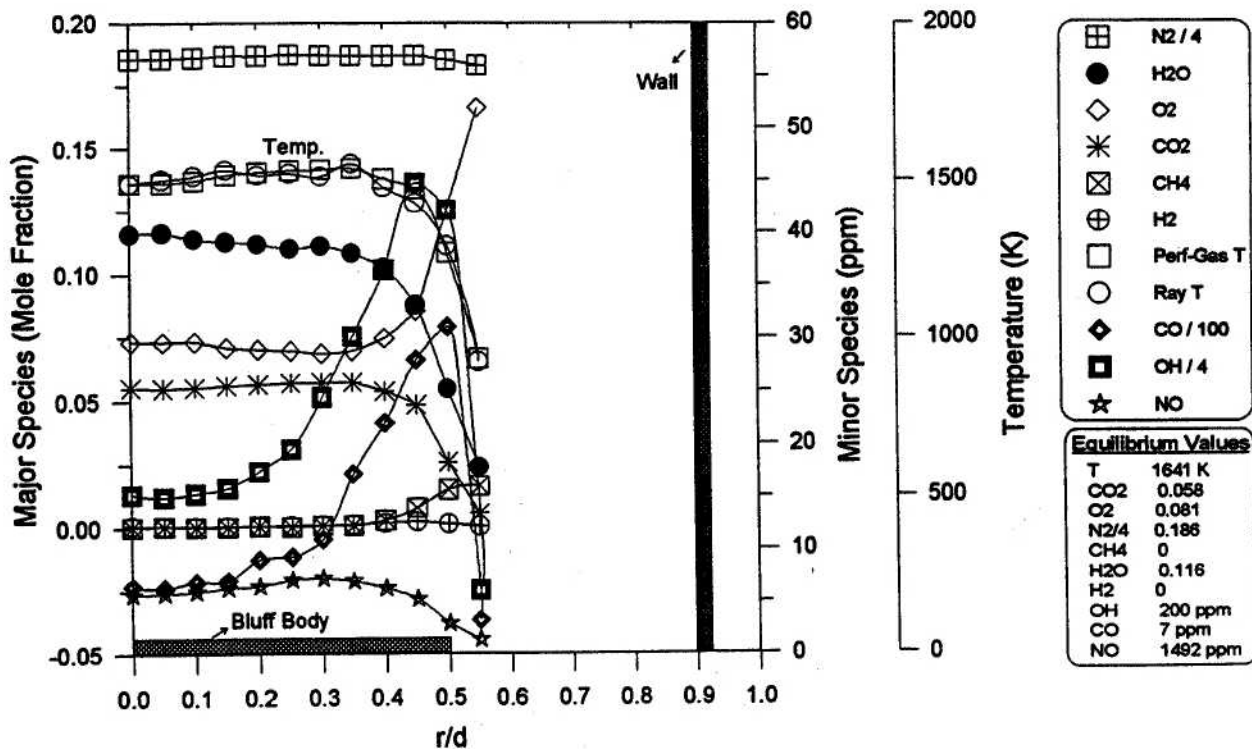


Fig. 14 Radial profiles of the mean species mole fractions and temperature at $x/d = 1.0$.

12-14. There are no significant differences in the species concentrations and temperature in the recirculation zone, when compared to their counterparts at $x/d = 0.1$ (see Fig. 7). The species concentrations and temperature are fairly uniform radially in the recirculation zone. The reaction progress variables (C) based on temperature at $x/d = 0.3, 0.6,$ and 1.0 are $0.91, 0.92,$ and 0.93 respectively. The constant reaction progress variable at all downstream locations in the recirculation zone indicates that the combustion in the recirculation zone is $\sim 90\%$ complete and the species and temperature are uniform in the entire recirculation zone. The downstream shear layer growth is seen from the broadening of the OH profiles of Figs. 7, 12-14. The shear layer growth is caused by the entrainment process, where isolated pockets of hot products (from the recirculation zone) and cold reactant gases (from the premixed fuel-air stream) are entrained into the shear layer. The CO profiles peak in the shear layer and the CO concentrations in the shear layer are 3-5 times the CO concentrations in the recirculation zone.

The mean radial profiles at the exhaust plane of the LP combustor ($x/d = 6.0$) are shown in Fig. 15. At this downstream location there has been sufficient time for the reactants to combine; the species concentrations and temperature correspond to the adiabatic equilibrium values. The OH concentrations increase gradually from the adiabatic equilibrium values (200 ppm) at the center ($r/d = 0$) and peak in the shear layer (~ 350 ppm). The CO concentrations increase from 750 ppm at $r/d = 0$ to 3000 ppm near the wall ($r/d = 0.8$). The increase in the CO concentrations is possibly due to the quenching from the cold wall. The average NO and CO concentrations (pollutants) in the exhaust plane as seen in Fig. 15 are ~ 6 ppm and ~ 740 ppm respectively

The instantaneous measurements at $x/d = 6$ and $r/d = 0$ (point A of Fig. 15) are shown in Fig. 16. The major species ($\text{CH}_4, \text{O}_2, \text{CO}_2,$ and H_2O), temperature and OH are at adiabatic equilibrium. The scatter plots of the major and minor species at $x/d = 6$ and $r/d = 0.8$ (point B

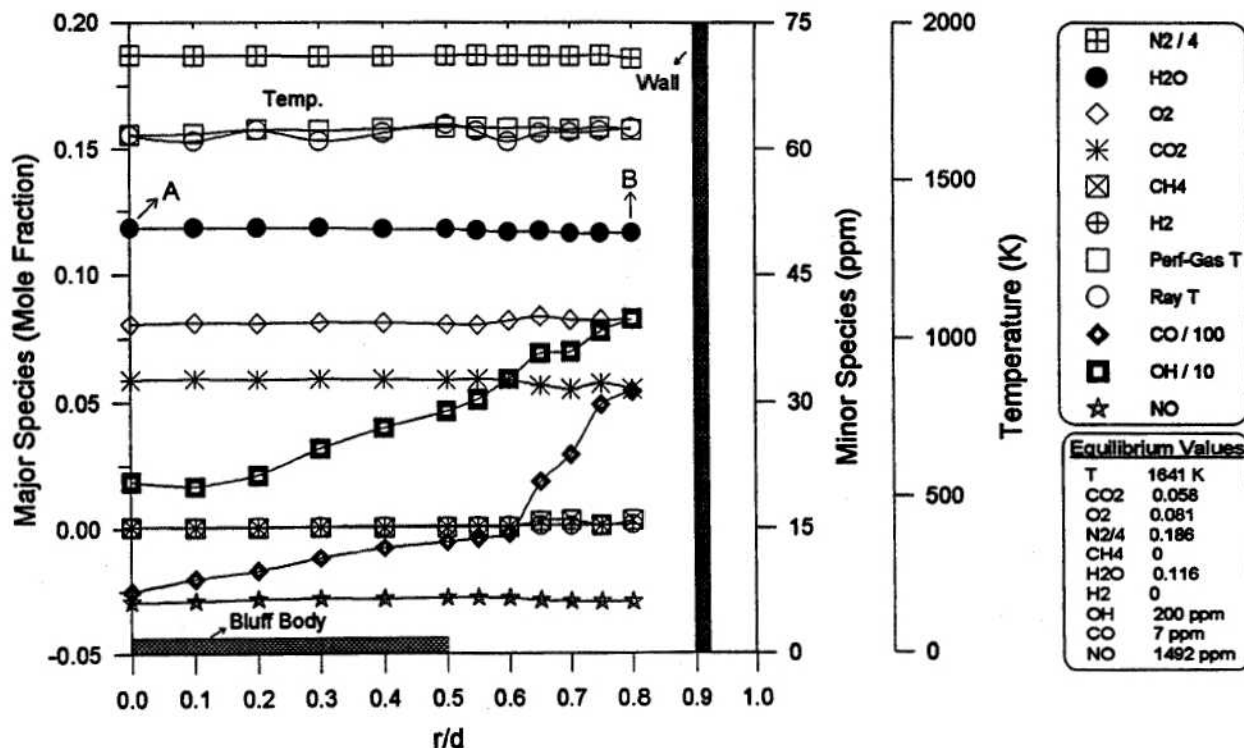


Fig. 15 Radial profiles of the mean species mole fractions and temperature at $x/d = 6.0$.

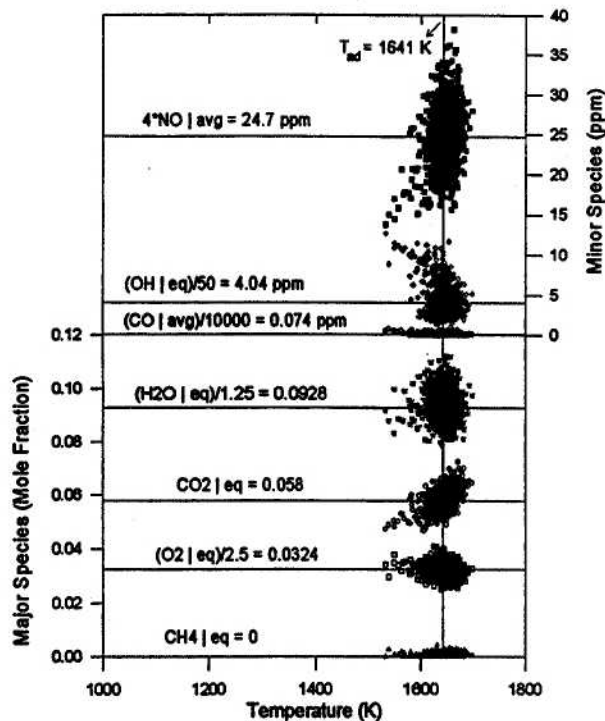


Fig. 16 Scatter plots of measured species mole fractions versus temperature in the combustor at $x/d = 6.0$ and $r/d = 0$ (Point A of Fig. 15). The equilibrium compositions of the major species and OH corresponding to an equivalence ratio of 0.586 are shown.

of Fig. 15), are shown in Fig. 17. The instantaneous measurements of Fig. 17 show methane mole fractions as high as 0.058 (the mole fraction of CH_4 in the premixed fuel/air stream), which indicates that a small amount of fuel leaks through the gap between the shear layer and the combustor wall, and exits the combustor unignited. This cold unignited fuel contributes to increased CO emissions near the combustor wall which is seen in Fig. 15 and could be due to the quenching from the cold wall. The single-shot CO concentrations as seen in Fig. 17 are as high as 1.7% (17,000 ppm). The average hydroxyl (OH) concentrations are at super equilibrium, and superequilibrium OH concentrations of upto 4 times (800 ppm) the equilibrium values are recorded.

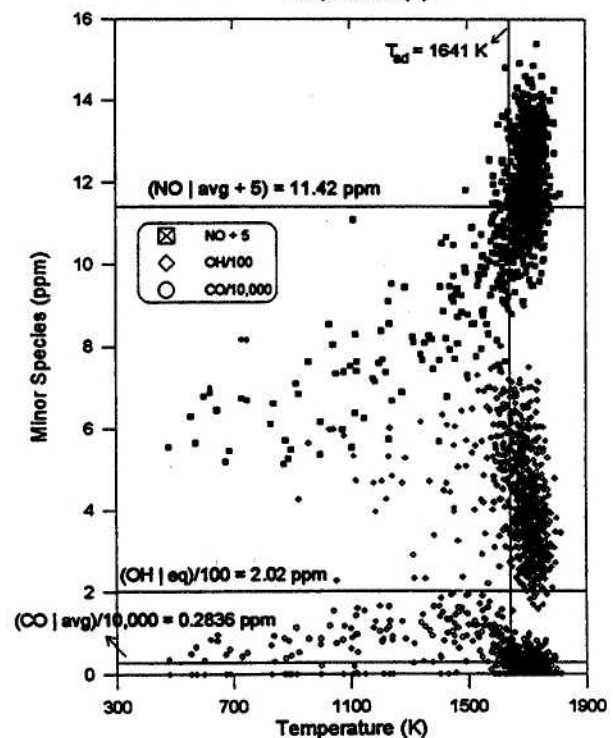
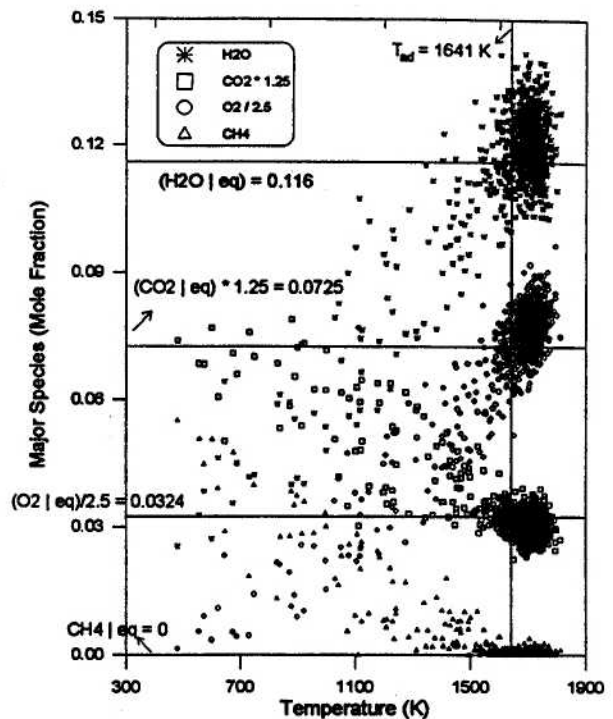


Fig. 17 Scatter plots of measured species mole fractions versus temperature in the combustor at $x/d = 6.0$ and $r/d = 0.8$ (Point B of Fig. 15). The equilibrium compositions of the major species and OH corresponding to an equivalence ratio of 0.586 are shown.

Probe Measurements

The exhaust pollutants (NO and CO) were also measured with gas sampling probes. The NO measurements were performed with a chemiluminescent gas analyzer, and CO was measured with an uncooled nondispersive infrared (NDIR) detector.²⁵ The gas samples were extracted from the exhaust plane of the combustor with 5 mm diameter probe. Optical and gas sampling probe measurements of the exhaust pollutants (NO and CO) at $x/d = 6$ are shown in Fig. 18. The laser based (LIF) NO measurements are

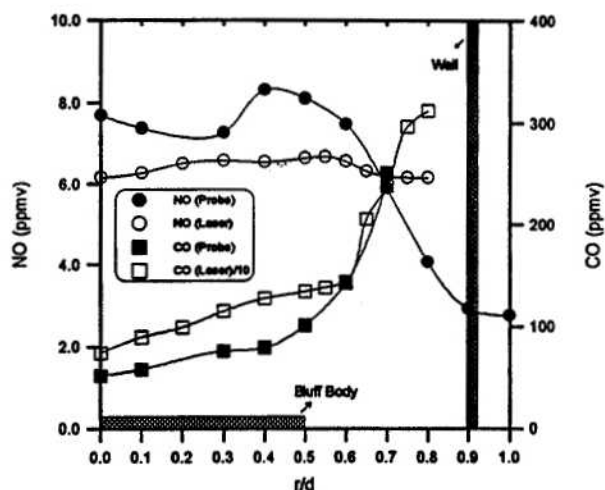


Fig. 18 Comparison of gas sampling probe measurements of exhaust pollutants (NO and CO) to laser measurements at $x/d = 6.0$.

in good agreement with the gas sampling probe measurements (within 2 ppm). However, the CO concentrations measured with the laser are about 10 times larger than the corresponding probe measurements. The reduced CO concentrations in the probe measurements are believed to be due to the oxidation of CO to CO₂ in the warmer sections of the uncooled probe via the reaction, $\text{CO} + \text{OH} \rightarrow \text{CO}_2 + \text{H}$. The oxidation of CO to CO₂ in gas sampling probes, resulting in a biased CO measurements with extraction probes have been reported by previous researchers.^{26, 27} In lean premixed flames where there are considerable CO concentrations, the extraction gas sampling probes can be increasingly inaccurate.

Conclusions

Simultaneous and instantaneous time-resolved point measurements of major species (CO₂, CH₄, H₂, O₂, N₂, and H₂O) concentrations, temperature, and minor species (CO, NO and OH) concentrations were obtained using a combination of spontaneous Raman scattering, Rayleigh scattering, and laser-induced fluorescence in a turbulent lean premixed methane combustor. The major species and CO were measured by spontaneous Raman scattering, temperature was determined by Rayleigh scattering, and the minor species (NO and OH) were measured with LIF. The fluorescence signals of NO and OH were corrected for Boltzman fraction and collisional quenching rates on a shot-to-shot basis.

Results show that the combustion in the recirculation zone is nearly complete and the reaction progress variable based on temperature is ~ 0.92 . The species concentrations and temperature are fairly uniform radially at all downstream locations in the recirculation zone of the combustor. The location and growth of the shear layer is determined from the OH profiles. In the shear layer, superequilibrium OH concentrations (upto 4 times the equilibrium values) are seen in the instantaneous measurements. The CO concentrations peak in the shear layer and the CO concentrations in the shear layer are about 3-4 times their corresponding values in the recirculation zone. The NO concentrations are fairly constant in the combustor and range from 3-10 ppm. In the exhaust plane of the combustor ($x/d = 6$), the species and temperature are near adiabatic equilibrium. Measurements of NO in the exhaust plane ($x/d = 6$) of the combustor revealed relatively low concentrations of NO (~ 6 ppm). The NO measurements reported here could be $\sim 2-3$ ppm higher than the actual values due to the unaccounted interference of O₂ on the NO channel. The CO concentrations in the exhaust were high ~ 1000 ppm. Single-pulse CO concentrations as high as 17,000 ppm are seen in the exhaust plane near the wall of the combustor.

The laser based measurements of the pollutants (NO and CO) in the exhaust plane of the combustor are compared with gas sampling probe measurements. The NO

measurements with both techniques agree with each other. However, the laser based measurements of CO are about 10 times larger than the gas sampling probe measurements. This suggests that the catalytic reactions (oxidation of CO to CO₂) in the probe make extraction probe techniques for CO measurement increasingly inaccurate in LP CH₄ flames.

Acknowledgments

The research at Vanderbilt University was funded by the U. S. Department of Energy Technology Center under Contract No. DE-FC21-92MC29061. The work at Sandia National Laboratories was supported by the United States Department of Energy, Office of Basic Energy Sciences. The authors would like to thank Dr. Mel Roquemore of Air Force Wright Laboratories, for lending the LP combustor. We would also like to acknowledge T. Prast for his assistance in the laboratory.

References

1. Magruder, T. D., McDonald, J. P., Mellor, A. M., Tanouchi, J., Nicol, D. G., and Malte, P. C., (1995) "Engineering Analysis for Lean Premixed Combustor Design," *31st AIAA/ASME/SAE/ASEE Joint Propulsion Conference, AIAA 95-3136*.
2. Pan, J. C., Vangsness, M. D., Heneghan, S. P., Schmoll, W. J., and Ballal, D. R., (1991) "Laser Diagnostic Studies of Confined Turbulent Premixed Flames Stabilized by Conical Bluff Bodies: Data Set," *University of Dayton Report, UDR-TR-91-102*, July.
3. Drake, M. C., Correa, S. M., Pitz, R. W., Shyy, W., and Fenimore, C. P., (1987) "Superequilibrium and Thermal Nitric Oxide Formation in Turbulent Diffusion Flames," *Combustion and Flame* 69, pp. 347-365.
4. Driscoll, J. F., Chen, R. H., and Yoon, Y., (1992) "Nitric Oxide Levels of Turbulent Jet Diffusion Flames: Effects of Residence Time and Damkohler Number," *Combustion and Flame* 88, pp. 37-49.
5. Vranos, A., Knight, B. A., Procia, W. M., Chiapetta, L., and Smooke, M. D., (1992) "Nitric Oxide Formation and Differential Diffusion in a Turbulent Methane-Hydrogen Diffusion Flame," *Twenty-Fourth Symposium (International) on Combustion*, The Combustion Institute, Pittsburgh, pp. 377-384.
6. Dibble, R. W., Masri, A. R., and Bilger, R. W., (1987) "The Spontaneous Raman Scattering Applied to Nonpremixed Flames of Methane," *Combustion and Flame* 67, pp. 189-206.
7. Dibble, R. W., Stårner, S. H., Masri, A. R., and Barlow, R. S., (1990) "An Improved Method of Data Acquisition and reduction for Laser Raman-Rayleigh and Fluorescence Scattering from Multispecies," *Applied Physics B* 51, pp. 39-43.
8. Mansour, M. S., Bilger, R. W., and Dibble, R. W., (1988) "Raman/Rayleigh and Mie-Scattering Measurements in a Reverse Flow Reactor Close to Extinction," *Twenty-Second Symposium (International) on Combustion*, The Combustion Institute, Pittsburgh, pp. 711-719.
9. Mansour, M. S., Bilger, R. W., and Dibble, R. W. (1990), "Turbulent Premixed Flames of Methane Near Extinction in a Reverse Flow reactor," *Second International Workshop on Turbulent Premixed Combustion*, CNRS, Paris.
10. Mansour, M. S., Bilger, R. W., and Dibble, R. W., (1991) "Turbulent Partially Premixed Flames of Nitrogen-Diluted Methane Near Extinction," *Combustion and Flame* 85, p. 215.
11. Masri, A. R., Bilger, R. W., and Dibble, R. W., (1987) "Fluorescence Interference with Raman Measurements in Nonpremixed Flames of Methane," *Combustion and Flame* 68, pp. 109-119.
12. Masri, A. R., Bilger, R. W., and Dibble, R. W., (1987) "Turbulent Nonpremixed Flames of Methane Near Extinction: Mean Structure from Raman

- Measurements," *Combustion and Flame* 71, pp. 245-266.
13. Masri, A. R., Bilger, R. W., and Dibble, R. W., (1987) "Turbulent Nonpremixed Flames of Methane Near Extinction: Probability Density Functions," *Combustion and Flame* 73, pp. 261-285.
 14. Stårner, S. H., Bilger, R. W., Dibble, R. W., and Barlow, R. S., (1990), "Piloted Diffusion Flames of Diluted Methane Near Extinction: Detailed Structure from Laser Measurements," *Combustion Science and Technology* 72, pp. 255-269.
 15. Pope, S. B., (1990) "Computations of Turbulent Combustion: Progress and Challenges," *Twenty-Third Symposium (International) on Combustion*, The Combustion Institute, Pittsburgh, pp. 591-612.
 16. Mansour, M. S., Bilger, R. W., and Stårner, S. H., (1989) "A Reverse Flow Reactor for Turbulence/Chemistry Interaction Studies," *Combustion Science and Technology* 65, pp. 83-101.
 17. Pan, J. C., Vangsness, M. D., Heneghan, S. P., and Ballal, D. R., (1991) "Scalar Measurements in Bluff Body Stabilized Flames Using CARS Diagnostics," *ASME Paper No. 91-GT-302*.
 18. Pan, J. C., Schmoll, W. J., and Ballal, D. R., (1992) "Turbulent Combustor Properties Behind a Confined Conical Stabilizer," *Transactions of ASME, Journal of Engineering for Gas Turbines and Power* 114, pp. 33-38.
 19. Pan, J. C., and Ballal, D. R., (1992), "Chemistry and Turbulence Effects in Bluff Body Stabilized Flames," *ALAA Paper No. 92-0771*.
 20. Gardiner, W. C., Hidaka, Y., and Tanzawa, T. (1981), "Refractivity of Combustion Gases," *Combustion and Flame* 40, pp. 213-219.
 21. Carter, C. D., and Barlow, R. S., (1994), "Simultaneous Measurements of NO, OH, and the Major Species in Turbulent Flames," *Optics Letters* 19, pp. 299-301.
 22. Barlow, R. S., and Carter, C. D., (1994) "Raman/Rayleigh/LIF Measurements of Nitric Oxide Formation in Turbulent Hydrogen Jet Flames," *Combustion and Flame* 97, pp. 261-280.
 23. Reynolds, W. C., (1986) "The Element Potential Method for Chemical Equilibrium Analysis: Implementation in the Interactive Program STANJAN," *Stanford University*.
 24. Reisel, J. R., Carter, C. D., Laurendeau, N. M., and Drake, M. C., (1993) "Laser-Saturated Fluorescence Measurements of Nitric Oxide in Laminar, Flat, C₂H₆/O₂/N₂ Flames at Atmospheric Pressure," *Combustion Science and Technology* 91, pp. 271-295.
 25. Kellor, J. O., Bramlette, T. T., Barr, P. K., and Alvarez, J. R., (1994) "NO_x and CO Emissions from a Pulse Combustor Operating in a Lean Premixed Mode," *Combustion and Flame* 99, pp. 460-466.
 26. Kramlich, J. C., and Malte, P. C., (1978) "Modeling and Measurement of Sample Probe Effects on Pollutant Gases Drawn from Flame Zones," *Combustion Science and Technology* 18, pp. 91-104.
 27. Nguyen, Q. V., Edgar, B. L., Dibble, R. W., and Gulati, A., (1995) "Experimental and Numerical Comparison of Extractive and In Situ Laser Measurements of Non-Equilibrium Carbon Monoxide in Lean-Premixed Natural Gas Combustion," *Combustion and Flame* 100, pp. 395-406.